Ab-initio and Continuum Simulation of High-Field Chemistry of Diphenylgermane and Diphenylsilane for Scanning Probe Direct Write

Wenjun Jiang
Department of Physics
Department of Electrical Engineering
University of Washington
Seattle, WA 98195, USA
wjjiang@uw.edu

Haoyu Lai
Department of Electrical Engineering
University of Washington
Seattle, WA 98195, USA

Marco Rolandi
Department of Materials Science and Engineering
University of Washington
Seattle, WA 98195, USA

Scott T. Dunham
Department of Electrical Engineering
Department of Physics
Department of Materials Science and Engineering
University of Washington
Seattle, WA 98195, USA

***Abstract*— We explore the localized synthesis of germanium and silicon nanostructures from organometallic liquid precursors under extremely high electric field (> 10^9 V/m) at a biased atomic force microscope (AFM) tip by coupling ab-initio and continuum electronic device simulation. We use the Sentaurus Device simulator (Synopsys®), adapted with material-specific models for diphenylgermane and diphenylsilane precursors, to explore the impact of high electric field on device behavior. High field at AFM tip causes the emission of electrons from the AFM tip via Fowler-Nordheim tunneling. We propose that some of the field emitted electrons pass directly into the substrate without interacting with the precursor molecules, while other electrons also drop into the LUMO of the precursor molecule and form a temporary negative ion (TNI), which, upon fragmentation, will result in the germanium / silicon nanostructures. We use ab-initio calculation package (VASP®) in order to calculate the influence of electric field on the shape of the HOMO of the precursor molecules. Finally, we built a more complicated model to explore the impact from Si / Ge deposition thickness on the charge carrier distribution.**

Keywords—ab-initio calculation; device simulation; Fowler-Nordheim tunneling; temporary negative ion

I. INTRODUCTION

Scanning probe-based techniques offer a novel solution to studying localized chemistry on the nanoscale. Due to their ability to apply a localized stimulus or reactant to a spatially confined area, scanning probes have been used to study chemistry for applications from lithography to catalysis.[1] Additionally, much focus on the past twenty years has been on the use of electric fields in conjunction with scanning probe lithography. External electric fields (EEFs) above a certain threshold can induce the rearrangement of electronic orbitals in atoms and molecules, thus inducing field-assisted chemical reactions.[2] The spatial confinement offered by scanning probe lithography offers a way to access electric fields of this magnitude on the nanoscale. SPL techniques using electric fields as a stimulus include electron-field induced transfer of tip coatings to a surface, electrochemical deposition from precursor solutions, and electrochemical dip-pen nanolithography. Electric fields have also been used in conjunction with scanning probe microscopy to locally oxidize Si, form carbonaceous deposits and etch resists, and recently, to direct write fabricate inorganic nanostructures using a biased AFM tip.[3]

The AFM direct write process uses low energy field emitted electrons to drive chemical reactions. A variety of techniques, including STM-induced CVD and electron beam induced deposition (EBID) also use low energy electrons to induce the deposition of inorganic nanostructures from inorganic precursors. In these two techniques, the precursor is normally in the gaseous form. While researchers have developed an understanding of silicon oxidation kinetics and have recently posited models for carbonaceous deposition from the gas phase,[4] an initial model for the direct write of inorganic nanostructures has only recently been suggested.[5] In this article, we propose reaction pathway which is the field emission of an electron from the AFM tip via Fowler-Nordheim tunneling.

II. AB-INITIO CALCULATION

A. Suggested Model

Since the electric field at the tip region of the atomic force microscopy is extremely high (> 1 V/nm at a moderate 10 V bias), the high E-field causes the emission of electrons from the AFM tip via Fowler-Nordheim tunneling. We propose that some of the field emitted electrons pass directly to the substrate

without interacting with the precursor molecules, while the other electrons drop into the LUMO of the precursor molecules and form a temporary negative ion (TNI), which upon further fragmentation will result in the germanium or silicon nanostructures. The TNI are attracted by the electric field gradient towards the tip-sample interface, as shown in Fig. 1.

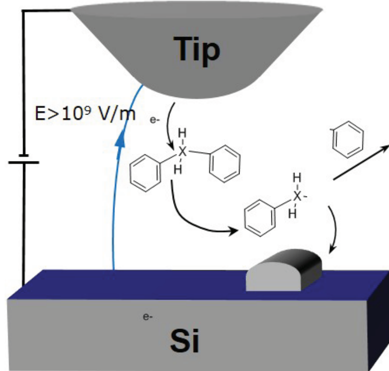

Fig. 1. AFM direct write schematic. This figure illustrates the charge carrier transport process between the AFM tip and the substrate.

B. Ab-initio Calculation

The DFT calculations are done using the Vienna Ab-initio Simulation Package (VASP)[6] with generalized-gradient approximation (GGA). The supercell size is 2.5nm x 2.5nm x 2.5nm with only one k-point sampling at Γ point. The calculation results are illustrated in Fig. 2.

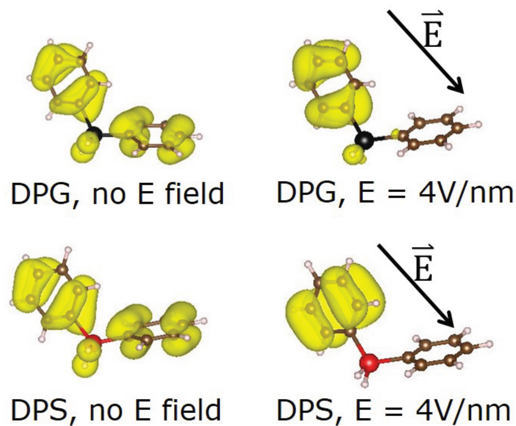

Fig. 2. VASP simulations of the HOMO with cell size 2.5 nm x 2.5 nm x 2.5 nm for DPG and DPS (a, c) with no external electric field and with an external electric field of 4 V/nm (b, d DPG and DPS, respectively). The direction of the electric field is indicated by the black arrow.

It is clear from Fig. 2 that the electric field influences the shape of the HOMO of the precursor molecules dramatically. In the absence of an electric field, the electron density of the HOMO is primarily distributed across the two phenyl groups, while with an applied electric field as strong as 4 V/nm, the electron density becomes confined to a single phenyl group.

C. Fowler-Nordheim Tunneling Model

High E-field causes the electrons in the silicon conduction band to see a triangular energy barrier, the width of which depends on the applied field, and the height of which is determined by the bandgap and electron affinity of silicon and SiO_2. The tunneling probability can be calculated by WKB approximation:

$$T = \frac{e^{-2\int_{x_1}^{x_2} dx \sqrt{\frac{2m}{\hbar^2}(V(x)-E)}}}{\left(1+\frac{1}{4}e^{-2\int_{x_1}^{x_2} dx \sqrt{\frac{2m}{\hbar^2}(V(x)-E)}}\right)^2}$$

$$\approx 16\frac{E}{U_0}\left(1-\frac{E}{U_0}\right)e^{-2L\sqrt{\frac{2m}{\hbar^2}(U_0-E)}} \quad (1)$$

And the tunneling current is therefore calculated by:

$$J = \alpha E_{inj}^2 exp\left(-\frac{E_c}{E_{inj}}\right) \quad (2)$$

where $\alpha = \frac{q^3}{8\pi\hbar\phi_b}\frac{m}{m^*}$, $E_c = 4\sqrt{2m^*}\frac{\phi_b^{3/2}}{3\hbar q}$ with ϕ_b=3.2eV is the energy barrier at injecting (Si-SiO_2) interface, E_{inj} is electric field at injecting interface, m=$1.6x10^{-19}$C for electron mass, and m*=0.42m for effective mass of an electron in the bandgap of SiO_2.

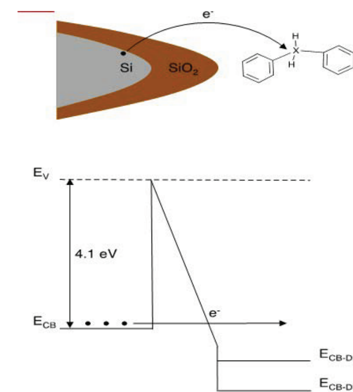

Fig. 3. Fowler-Nordheim tunneling process schematic. The applied electric field lowers the barrier for an electron in the Si to tunnel through the potential barrier of the oxide.

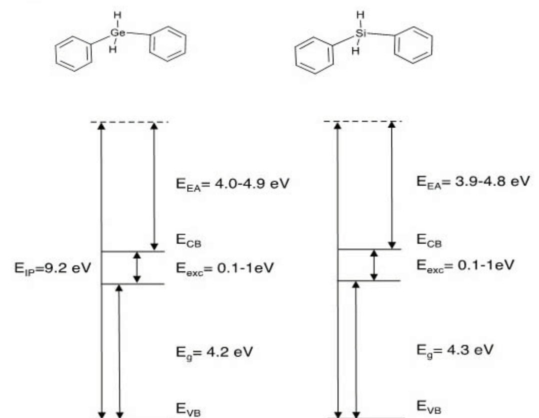

Fig. 4. The HOMO and LUMO levels of DPG (left) and DPS (right) molecules, which are determined by UV-Vis spectroscopy and literature research.

In our case, the extremely high E-field causes the width of the barrier to become small enough so that electrons can tunnel through the barrier from the silicon conduction band into the oxide conduction band, as illustrated in Fig. 3.

There is no published data for the precise position of the HOMO and LUMO levels of DPS and DPG. We used the published data for ionization potential (IP), together with experimentally measured optical band gap of DPS and DPG molecules, to estimate the HOMO and LUMO levels. The detailed data are shown in Fig. 4.

D. Device Simulation

Simulations of fields and current in the tip/liquid/substrate system are conducted using the Sentaurus Device Simulator® [7] from Synopsys. The AFM tip is very heavily Sb doped (about 10^{20} cm^{-3}) n-type Silicon with a radius of curvature equal to 15 nm capped by a conformal 2 nm layer of SiO_2. The p-type silicon substrate is heavily boron doped (10^{19} cm^{-3}) with a uniform 2 nm layer of SiO_2. The tip and substrate is nearly in contact (3 Å). The surrounding region is filled with the precursor liquid, which is modeled as a semiconductor with very low ionic mobility on the order of 10^{-6} $cm^2/(V{\cdot}s)$, as illustrated in Fig. 5.

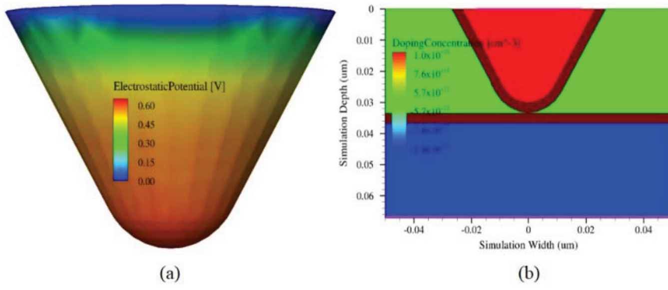

Fig. 5. (a) 3D electrostatic potential plot of AFM tip, with 15 nm radius; (b) Cross-section plot of device simulation setup, with AFM tip doped with 10^{20} cm^{-3} Antimony and silicon substrate doped with 10^{19} cm^{-3} Boron, both of which are covered by ~2 nm SiO_2.

We utilize a phonon-assisted tunneling model based on the work of Schenk *et al*, non-local tunneling model for negatively charged ions in the liquid, together with current continuity equations that are solved consistently with Poisson equation. The simulations are based on a 2D system with a depth of 20 nm chosen based on the lateral current distribution used on calculate total tip current. The parameter values employed for DPG/DPS are $\varepsilon_{DPG} = \varepsilon_{DPS} = 2.5$, $\chi_{DPG} = 4.0$ eV, $\chi_{DPS} = 4.0$ eV, $Eg_{DPG} = 4.2$ eV, $Eg_{DPS} = 4.3$ eV.

III. Results

A. High Electric Field Concentration at AFM Tip Region

The extremely high electric field concentrates at the tip region of atomic force microscope, due to the small radius of highly doped silicon tip. As shown in Fig. 6, the electric field can easily exceeds 10^9 V/m at a moderate external applied voltage at 10 V.

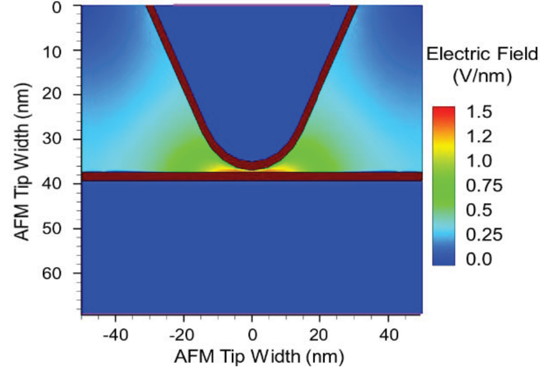

Fig. 6. Cross section of the high electric field concentration at 10 V.

B. Current-Voltage Curve

We can precisely match the current-voltage (I-V) plots with experimental results. As illustrated in Fig. 7, the on-set voltage for DPG is about 7±2 V, while the current for DPS liquid doesn't increase dramatically until the applied voltage is higher than 9±2 V. The difference in onset voltages indicates that higher energy may be required for TNI formation of the DPS molecule.

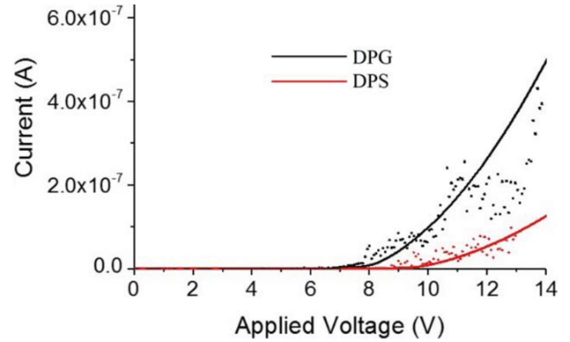

Fig. 7. DPG and DPS I-V characteristics.

C. Deposition Rates at Different Biases

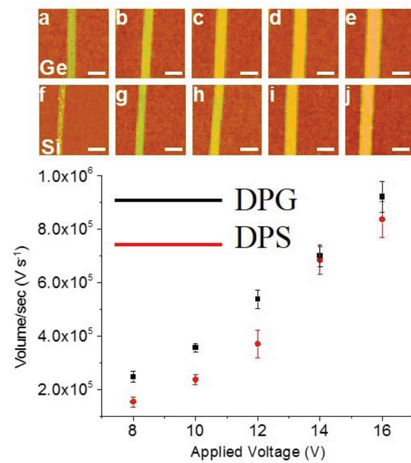

Fig. 8. AFM direct-write deposition rate comparison for DPG and DPS.

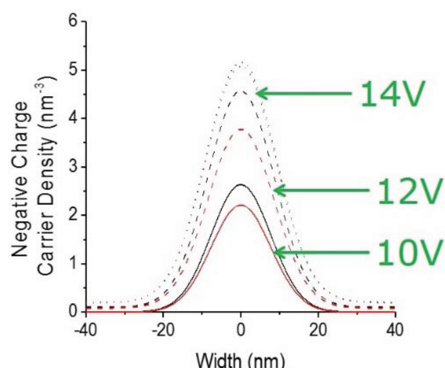

Fig. 9. AFM direct-write charge carrier density distribution comparison for DPG (black) and DPS (red) at 10 V (solid), 12 V (dashed) and 14 V (dotted).

The most useful application for AFM direct write is its capability of depositing Si / Ge in lines with ultra-thin width. Here we model the Si / Ge deposition rate with a moving AFM tip at slow constant speed (~ 1 μm/s) at different applied voltages (8V, 10V, 12V, 14V, and 16V). The calculation matches well with experimental result, as shown in Fig. 8 and Fig. 9.

D. *Impact from Deposition Thickness*

Based on Fig. 9, we established further models to investigate the impact from deposited Si / Ge nanostructure on the charge carrier density. We insert an ultra-thin layer of Si / Ge between AFM tip and SiO_2 on substrate, as shown in Fig. 10.

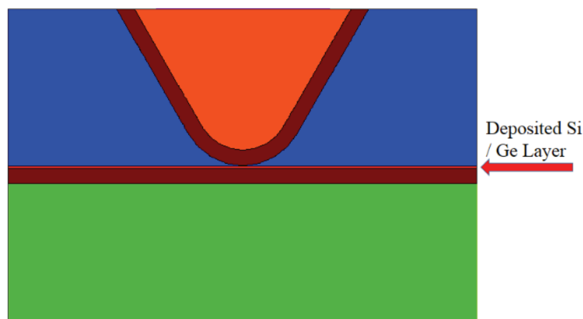

Fig. 10. Si / Ge deposited on SiO2 layer of the substrate.

The peak value of negative charge carrier density (value at width = 0 nm in Fig. 9) as a function of deposited thickness is illustrated in Fig. 11. The peak value shows a clear negatively linear dependence on deposition height.

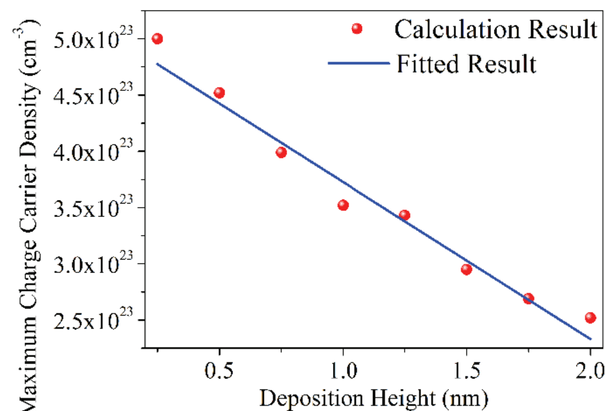

Fig. 11. Peak value of negative charge carrier density *vs.* deposition height for DPG at applied voltage = 14V.

IV. Conclusion

We have built a model coupling ab-initio calculation with device simulation to study the AFM direct write at extremely high electric field. VASP calculation demonstrates obvious impact from applied bias on the charge density distribution on DPG / DPS molecules. Using Sentaurus device simulator, we precisely matched the I-V plots and deposition rate results with experiments, and plotted the charge carrier density distribution at different biases. We then established a more complicated model that includes the deposited Si / Ge on substrate to explore the impact from deposition thickness on the charge carrier distribution. This model serves as a framework for controlling the deposition rate, width, and thickness of Si / Ge direct write via atomic force microscope.

References

[1] K. L. Yeung, and N. Yao, "Scanning Probe Microscopy in Catalysis," J. Nanosci. Nanotechnol. 4, pp. 647-690 (2004).

[2] H.J. Kreuzer, "Physics and Chemistry in High Electric Fields," Surf. Sci. 246, pp. 336-347 (1990).

[3] S.E. Vasko, A. Kapetanovic, V. Talla, M.D. Brasino, Z. Zhu, A. Scholl, J.D. Torrey, and M. Rolandi, "Serials and Parallel Si, Ge, and SiGe Direct-Write with Scanning Probes and Conducting Stamps," Nano. Lett. 11, pp. 2386-2389 (2011).

[4] J. Lee, D.C. Sorescu, and X.Y. Deng, "Electron-Induced Dissociation of CO2 on TiO2 (110)," J. Am. Chem. Soc., 2011, 133 (26), pp. 10066-10069.

[5] S.E. Vasko, W.J. Jiang, R.Y. Chen, R. Hanlen, J.D. Torrey, S.T. Dunham, and M. Rolandi, "Insights into Scanning Probe High-Field Chemistry of Diphenylgermane," Phys. Chem. Chem. Phys. 2011, 13, pp. 4842-4845.

[6] http://cms.mpi.univie.ac.at/vasp/vasp/

[7] Sentaurus Device User Manual, Version H-2013.03 (Synopsis Inc., Mountain View, CA, 2013)